

## Research on vibration characteristics of no-tillage seeding unit based on the MBD-DEM coupling

Dong He<sup>a,b</sup>, Hongwen Li<sup>a,b,\*</sup>, Jin He<sup>a</sup>, Caiyun Lu<sup>a</sup>, Chao Wang<sup>a</sup>, Yingbo Wang<sup>c,d</sup>, Zhengyang Wu<sup>a</sup>, Zhenwei Tong<sup>a</sup>, Zhen Gao<sup>a</sup>

<sup>a</sup> College of Engineering, China Agricultural University, Beijing 100091, China

<sup>b</sup> Key Laboratory of Agricultural Equipment for Conservation Tillage, Ministry of Agricultural and Rural Affairs, China

<sup>c</sup> College of Biosystems Engineering & Food Science, Zhejiang University, Hangzhou 310058, China

<sup>d</sup> School of Computer & Computing Science, Hangzhou City University, Hangzhou 310015, China

### ARTICLE INFO

#### Keywords:

Vibration model  
MBD-DEM  
Furrowing operations  
Vibration characteristics  
Vibration damping system

### ABSTRACT

Complex field conditions in conservation tillage significantly enhance the vibration of no-tillage planters, which is even more intense at high velocity, limiting the development and promotion of no-tillage seeding of high-speed precision technology. At present, it is difficult to understand the vibration characteristics of no-tillage planters, and how to reduce the influence of vibration on furrowing quality is still a critical problem. In this study, a depth-limiting vibration model of the no-tillage seeding unit (NTSU) was established based on the nonlinear continuous contact force model and dynamic analysis. The cone index test was used to calibrate DEM parameters for modeling the simulated soil, which was used to study the effect of soil compaction on the vibration of no-tillage unit. The multibody dynamics (MBD) and discrete element method (DEM) coupled simulation technology of coupled furrowing operation was proposed as the test vibration analysis method. The effects of the working velocity, the spring stiffness coefficient (SSC), and the cone index on the vibration characteristics of the NTSU were studied through orthogonal tests and analysis. The simulation and field test results show that the working velocity is the primary influence factor of the vibration of the no-tillage planter, but it is also affected by the downforce and soil compactness. The maximum amplitude increased as the working velocity increased, but the main frequencies of the vibration are concentrated in a low frequency band from 2 to 10 Hz. Reasonable working velocity and SSC (downforce) settings can effectively reduce the vibration of the NTSU and improve the quality of seeding. To sum up, this paper proposed a new method that can effectively and precisely simulate the furrowing operation, and study the influence of NTSU structure on its vibration. It would provide a theoretical basis for the optimization design of the vibration damping system.

### 1. Introduction

Conservation tillage is an advanced agricultural farming technology that can reduce soil erosion and improve soil fertility and drought resistance by eliminating traditional tillage, using minimal tillage, no-tillage, and straw mulching (Kassam,2015; Amir Kassam,2009). The no-tillage planter could perform seeding operations without significant soil disturbance, where soil surface undulations and crop residues could cause significant random vibrations in the seeding unit, and the random vibration could negatively affect the stability of the seed implantation and the crop yield (Cay et al., 2018; Liu et al., 2015). The no-tillage seeding unit (NTSU) is a critical working part of a no-tillage planter.

Therefore, studying the vibration characteristics of the NTSUs and reduce the influence of vibration on seeding quality is essential

In previous studies, researchers mainly obtained the vibration characteristics of the planter during field test, then the effect of vibration on seeding quality was studied (Badua et al., 2021; Sharipov et al., 2018; Virk et al., 2021; Zhai et al., 2020). Zhang et al. (2014) established a two-degree-of-freedom spade planter vibration model which can be used to predict and analyze the seeding performance of the spade punch planter under the working operations. By testing and analyzing the vibration characteristics of the no-tillage planter during the field test, Zhang et al. (2016) studied the influence law of vibration parameters of seed metering device on corn population movement in seed metering device based on DEM; Wang et al. (2019) built a test bench for vibration

\* Corresponding author.

E-mail address: [lhwen@cau.edu.cn](mailto:lhwen@cau.edu.cn) (H. Li).

<https://doi.org/10.1016/j.compag.2024.109877>

Received 26 May 2024; Received in revised form 1 November 2024; Accepted 23 December 2024

Available online 13 January 2025

0168-1699/© 2024 Elsevier B.V. All rights are reserved, including those for text and data mining, AI training, and similar technologies.

Nomenclature			
<b>Symbols</b>		$n$	The elastic contact index (generally 1.5 for steel)
$C_r$	The collision coefficient of restitution.	<b>Greek Letters</b>	
$D$	The damping factor	$R$	The equivalent contact radius of colliding bodies (m)
$E$	The equivalent Young's modulus of colliding bodies (Pa)	$R_b, R_j$	The contact radius of colliding bodies (m)
$E_b, E_j$	The Young's modulus of colliding bodies (Pa)	$\nu_b, \nu_j$	The Poisson's ratio of colliding bodies (m/s)
$F_c$	The contact force(N)	$v_{1i}, v_{2i}$	The initial velocity of colliding bodies (m/s)
$F_g$	The vertical force resistance of the ground on the GW (N)	$v_{1j}, v_{2j}$	The final velocity of colliding bodies (m/s)
$F_r$	The horizontal resistance of the ground on the GW (N)	$\alpha$	The recovery factor
$g$	the acceleration of gravity ( $m/s^2$ )	$\delta$	The relative penetration (m)
$J$	The rotational inertia of the depth limiting device ( $kg \cdot m^2$ )	$\cdot\delta \cdot \delta$	The penetration velocity (m/s)
$J_1$	The rotational inertia of the GWSA ( $kg \cdot m^2$ )	$\theta \cdot \delta^{(-)}$	The initial relative normal contact velocity(m/s)
$J_2$	The rotational inertia of the depth-limiting adjustment handle ( $kg \cdot m^2$ )	$\theta$	The angle between the GWSA and the frame ( $^\circ$ )
$K$	The Hertz contact stiffness (N/m)	$\cdot\cdot\theta$	The second-order differentiation of the $\theta$ ( $^\circ/s^2$ )
$L_0$	The length of the GWSA (m)	$\chi$	The hysteresis damping factor
$L_1$	The length of $F_c$ force arm	$\cdot\cdot\delta$	the second-order differentiation of the $\delta$ ( $m/s^2$ )
$m$	The contact parameter	<b>Abbreviations</b>	
$M$	The sum of external moments on O point	RecurDyn	Recursive Dynamic
$m_0$	The equivalent mass of colliding bodies i, j (kg)	DEM	Discrete Element Method
$m_1$	The mass of the GWSA (kg)	GWSA	Gauge wheel support arm
$m_2$	The mass of the GW (kg)	DLAH	Depth-limiting adjusting handle
$m_i, m_j$	The mass of colliding bodies i, j (kg)	NTSU	No-tillage seeding unit
		SSC	Spring stiffness coefficient

seeding, which analyzed the effect of the field vibratory excitation on the finger-clamped seed metering device. The planter vibration increased linearly with increasing working velocity, but a reasonable selection of downforce size could attenuate seeder vibration. Zhai et al. (2020) quantified the effects of working velocity and seeding unit vibration on seeding quality by monitoring vibration at different working velocities and measuring plant spacing after emergence in a field test. Badua et al. (2021) investigated the variation coefficient of seeding depth at different working velocity and downforce settings (620 N and 980 N), and found that the target seeding depth could be achieved with reasonable downforce settings. In summary, vibration has a severe impact on seeding depth, which directly affects the seeding quality (Kirkegaard Nielsen et al., 2017), and the furrowing operation of “furrowing – depth limitation – profiling” process is a crucial factor affecting the seeding depth. However, there is a lack of research on the impact of the NTSU on vibration, especially the contact collision behavior between the gauge wheel support arm (GWSA) and the depth-limiting adjusting handle (DLAH) in the process of depth-limiting, which produces a violent impact force and intensifies the vibration of the NTSU. Therefore, it is necessary to understand the interaction mechanism between soil and the NTSU.

The simulations have already been used to analyze soil-agricultural tool interaction with passive vibration. Páthy et al. (2024) developed a two-way coupled DEM-FEM simulation procedure that can be applied to model the interaction between deformable tillage tools and the soil, as well as modeling the passive vibration of tillage tools in the soil. Galibjon M. Sharipov et al. (2017) developed a sensor frame for obtaining field surface profiles during seeding operation. They assessed and optimized the dynamic response of a no-till seeder and thus developed a mathematical model of the coulter assembly with the semi-active MR damper system. To date, however, based on our review of the literature, there have been no examples of the application of MBD-DEM simulations to passive vibration, which caused soil-agricultural tool interaction.

In this study, an MBD-DEM coupling simulation model was constructed to analyze the vibration characteristics of the NTSU based on the working velocity, spring stiffness coefficient (SSC), and cone index during the furrowing operation. The specific objective was to investigate

the vibration characteristics of the NTSUs. A depth-limiting vibration model of NTSU was established based on the nonlinear continuous contact force model and dynamic analysis. The cone index test was used to calibrate DEM parameters for modeling the simulated soil. The MBD-DEM simulation test of coupled furrowing operations was conducted to analyze the effects of working velocity, SSC, and cone index on the vibration of the NTSU. Furthermore, the feasibility and effectiveness of coupling model were verified through comparisons between simulation and field test.

## 2. Materials and methods

### 2.1. Depth-limiting vibration model of the NTSU

#### 2.1.1. Structure and working principles

The center of mass of the simplified no-tillage unit is in the frame as shown in Fig. 1, which is mainly composed of the four-bar profiling device, the stubble breaking and trenching device, the fertilizing device, the frame, the suppression device, the GWs, the double disc furrow openers, and other devices. The structure of the NTSU was moderately simplified, and the power transmission system, the seed metering device were removed.

During the operation of the no-tillage seeding unit, the stubble breaking and trenching device cuts through the stubble and soil. The double disc furrow openers are driven into the soil by their weight and the profiling spring downforce, and the two discs roll forward to furrow open the soil and form the seed furrow. The parallel four-bar profiling device realizes the up-and-down profiling function due to the uneven ground surface, straw, and soil resistance change. The depth-limiting device mainly utilizes the frame and DLAH to constrain the rotation angle of the GWSA, and adjusts the height of the DLAH by adjusting the position of the DLAH to achieve the limiting function and improve the adaptability to different soil height changes, and suppression device carry out soil backfilling and covering of the straw.

#### 2.1.2. Nonlinear continuous contact force model

The most common behavior in mechanical systems is the contact behavior, which is essential for the relevant analytical calculations in

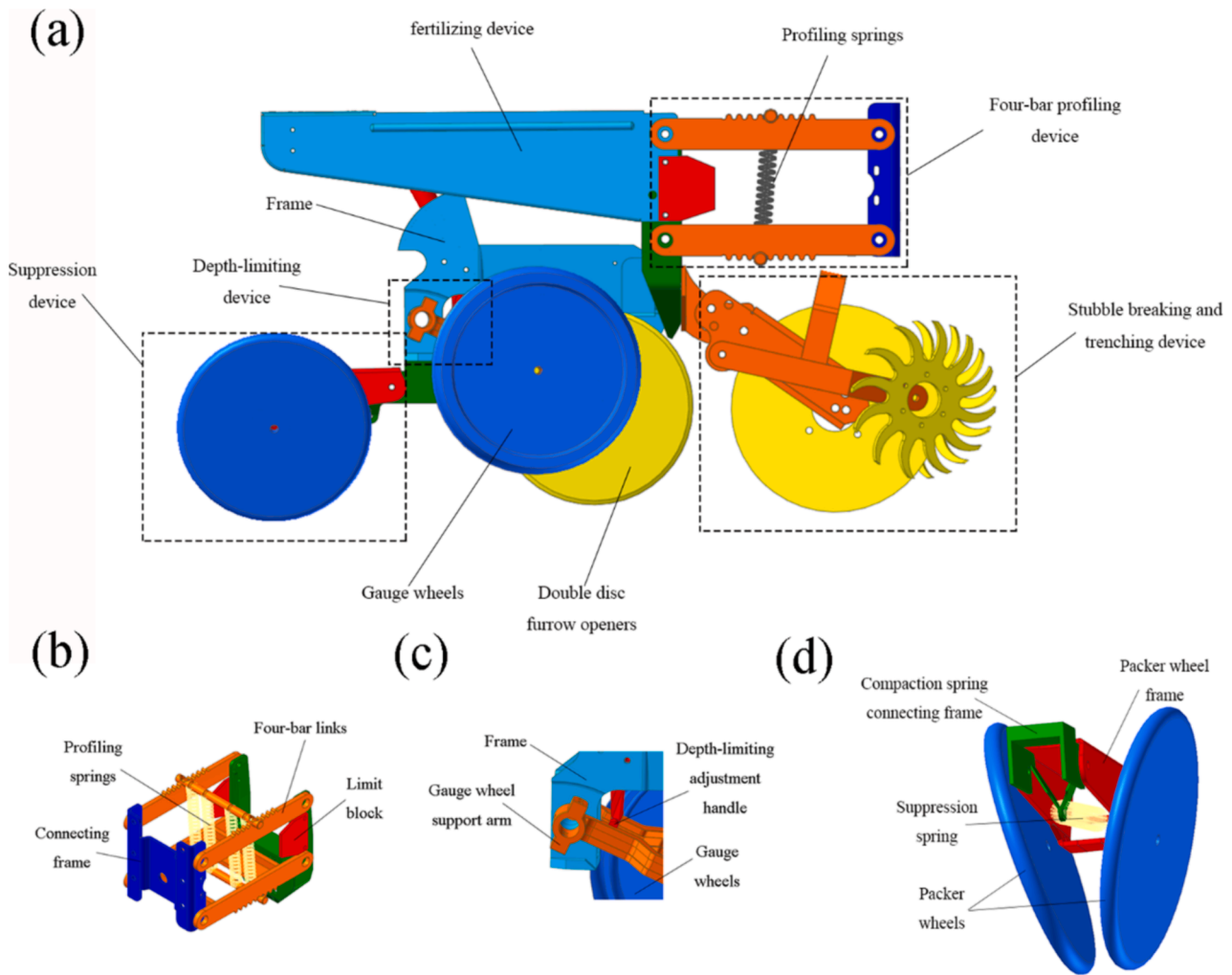


Fig. 1. Structure of no-tillage seeding unit. (a) Schematic diagram of the assembly position of no-tillage unit; (b) (c) (d) Structure of four-bar profiling device, depth-limiting device, and suppression device, respectively.

mechanical systems. The regularization method is applied in RecurDyn (Recursive Dynamic, FunctionBay, Korea) to describe the collision body contact behavior, which considers that each contact region of a contact body is covered with several spring damping elements dispersed on the surface (Rodrigues Da Silva et al., 2022). The magnitude of the deformations and stiffnesses of the elements depends on the geometric and material properties of the collision body as well as on the relative depth of penetration (Skrinjar et al., 2018; Zhang et al., 2022).

RecurDyn and EDEM used the Hertz contact force model to express the contact between two objects (Rodrigues Da Silva et al., 2022; Tsuji et al., 1992), where the contact force  $F_c$  is a nonlinear function of the amount of deformation:

$$F_c = K\delta^n \quad (1)$$

where  $\delta$  is the contact deformation;  $n$  is the energy index, which depends on the geometry of the contact material, and for metal contact, the value of  $n$  is taken as 1.5 (R. Ramirez et al., 1999);  $K$  is the Hertz contact stiffness (N/m), which is related to the elastic modulus of the two contacting materials, the contact radius and the Poisson's ratio (Wang & Liu, 2020), and its expression is:

$$K = \frac{4}{3}E^*\sqrt{R} \quad (2)$$

$$R = \sqrt{\frac{R_i R_j}{R_i \pm R_j}} \quad (3)$$

$$E^* = \frac{E_i E_j}{E_j(1 - \nu_i) + E_i(1 - \nu_j)} \quad (4)$$

where  $E^*$  is the equivalent Young's modulus of colliding bodies (Pa),  $E_i$  and  $E_j$  are the Young's moduli of the colliding bodies,  $R$  is the equivalent contact radius of colliding bodies (m),  $R_i$  and  $R_j$  are the radius of the colliding bodies, and  $\nu_i$  and  $\nu_j$  are the Poisson's ratios of the colliding bodies.

In order to describe the energy dissipation during the collision, Kelvin and Voigt created the K-V model in 1960 (Machado et al., 2012); while considering the shortcomings of the K-V model, Hunt and Crossley proposed a new model related to the relative velocity at the moment of collision in 1975 (Hunt and Crossley, 1975):

$$F_c = K\delta^n + \chi\delta^m \dot{\delta} \quad (5)$$

where  $m$  is the contact parameter, generally taken as 1.5;  $\chi$  is the hysteresis damping factor; and  $\dot{\delta}$  is the penetration velocity.

The hysteresis damping factor is:

$$\chi = \frac{3K(1 - C_r)}{2\dot{\delta}^{(-)}} \quad (6)$$

where  $C_r$  is the collision coefficient of restitution,  $\dot{\delta}^{(-)}$  is the initial relative normal contact velocity (m/s).

The collision coefficient of restitution is:

$$C_r = -\frac{v_{1j} - v_{2j}}{v_{1i} - v_{2i}} = -\frac{\dot{\delta}}{\dot{\delta}^{(-)}} \quad (7)$$

where  $v_{1i}$ ,  $v_{2i}$  is the initial velocity of colliding bodies (m/s),  $v_{1j}$ ,  $v_{2j}$  is the final velocity of colliding bodies (m/s).

The vibration equation for nonlinear collision behavior is:

$$m_0\ddot{\delta} + D\dot{\delta} + K\delta^3 = 0 \quad (8)$$

where  $\ddot{\delta}$  is the second-order differentiation of the  $\delta$  ( $m/s^2$ ),  $m_0$  is the equivalent mass of colliding bodies (kg), and  $D$  is the damping factor (N/m), which are expressed as:

$$m_0 = \frac{m_i + m_j}{m_i m_j} \quad (9)$$

$$D = \alpha(m_0 K)^{\frac{1}{2}} \delta^{\frac{1}{4}} \quad (10)$$

where  $m_i$  and  $m_j$  are the mass of colliding bodies (kg), and  $\alpha$  is the recovery factor,  $\alpha = \sqrt{\frac{5\ln^2 C_r}{\pi^2 + \ln^2 C_r}}$ , Therefore, the nonlinear continuous contact force model based on Hertz theory is:

$$F_c = K\delta^{\frac{3}{2}} + \alpha\sqrt{m_0 K} \delta^{\frac{1}{4}} \quad (11)$$

### 2.1.3. Vibration model of depth limits

During the operation of the depth limiting device, due to the inhomogeneity of the soil, the load on the depth limiting wheel was mainly due to the downforce and the horizontal resistance. In the kinetic study of the “furrowing – depth limiting – profiling” process, the vibration of the depth limiting device in the vertical direction was mainly analyzed, which was manifested in the contact collision behavior between the arm of the wheel and the depth limiting adjusting handle directly. In the contact collision modeling of the depth limiting device, ignoring the friction at the articulation on the movement of the GWs. The collision behavior was equivalent to a single degree of freedom spring-damping model, whose stiffness coefficients and damping coefficients were recorded as  $K$  and  $D$ , respectively. So that the depth-limiting vibration model of NTSU was shown in Fig. 2.

According to the combined moment theorem, the sum of the external moments on point O is:

$$M = F_g L_0 \cos\theta - F_c L_1 - F_r L_0 \sin\theta - \left(m_2 + \frac{m_1}{2}\right) g L_0 \cos\theta \quad (12)$$

where  $M$  is the sum of external moments on O point;  $F_c$  is caused by the collision of the GWSA and the DLAH;  $F_g$  and  $F_r$  are the vertical and horizontal resistance of the ground on the GW (N),  $L_0$  is the length of the GWSA (m),  $m_1$  is the mass of the GWSA (kg),  $m_2$  is the mass of the GW (kg),  $\theta$  is the angle between the GWSA and the frame ( $^\circ$ ),  $g$  is the acceleration of gravity ( $m/s^2$ ).

According to the momentum moment theorem, the kinetic equation is established:

$$J\ddot{\theta} + K\delta L_1 + D\dot{\delta} L_1 = M \quad (13)$$

where  $J$  is the rotational inertia of the depth limiting device ( $kg \cdot m^2$ ),  $L_1$  is the length of  $F_c$  force arm (m).

The moment of inertia  $J$  is:

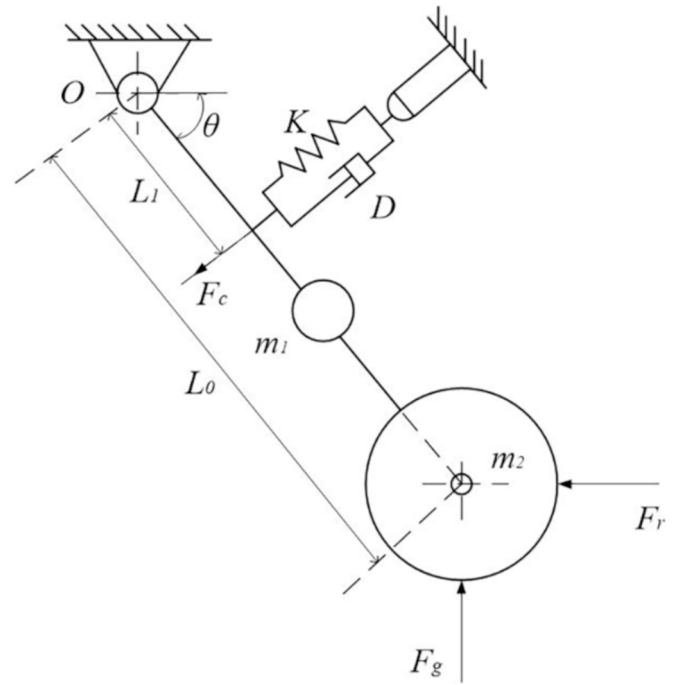


Fig. 2. Vibration model of depth limits.

$$J = \left(J_2 + m_2 L_0^2 + J_1 + \frac{m_1 L_0^2}{4}\right) \ddot{\theta} \quad (14)$$

where  $J_2$  is the moment of inertia of the GW ( $kg \cdot m^2$ ),  $J_1$  is the moment of inertia of the GWSA ( $kg \cdot m^2$ ),  $\ddot{\theta}$  is the second-order differentiation of the  $\theta$  ( $^\circ/s^2$ ).

The product of the second-order differential of contact deformation and the force arm  $F_c$  is:

$$\ddot{\theta} = \delta L_1 \quad (15)$$

This can be obtained by substituting equations (12), (14) and (15) into equation (12), which is a second order differential equation. It is a typical single degree of freedom vibration equation, which provides a theoretical basis for the MBD-DEM simulation:

$$\left(J_2 + m_2 L_0^2 + J_1 + \frac{m_1 L_0^2}{4}\right) \delta L_1 + D \dot{\delta} L_1 + K \delta L_1 = F_g L_0 \cos\theta - F_c L_1 - F_r L_0 \sin\theta - \left(m_2 + \frac{m_1}{2}\right) g L_0 \cos\theta \quad (16)$$

Associative (11), (16) that is, the depth limiting device vibration model, the contact force  $F_c$  will be affected by the relative collision speed, the vertical resistance  $F_g$  on the GW, and the weight of the NTSU. However, the vertical resistance  $F_g$  is mainly derived from the dead-weight of the NTSU and the downforce exerted by the profiling spring, so it is necessary to analyze the effect of working velocity and the profiling SSC on the vibration characteristics of the seeding unit. The impact of cone index as a measure of soil compactness affects plant growth and crop yield. At the same time, cone index, as an indicator of the degree of soil compactness, affects plant growth and crop yield. Therefore, its influence on the vibration characteristics of the NTSU should be further studied.

## 2.2. Calibration of the DEM parameters of soil

### 2.2.1. Properties of soils

The experimental field was loam soil on the soil bin performance test

bench of China Agricultural University. Five samples of soils were taken from the area that would be used for the no-tillage seeding test, and their physical properties were listed in Table 1. All sampling locations were on the sowing row, as this was about to be the subsequent crop row and the main source of the vibration for the seeding unit. The water content, the bulk density, and the dry density were measured from the cylindrical samples in their original state. The cone index was measured by a SC-900 cone penetration meter with a vertical velocity of approximately 30 mm/s, where the cone had a top angle of 60° and a diameter of 12.83 mm. For considering that maize seeds would be sown at a depth of 50–80 mm, the cone index of each sample area was measured up to a depth of 100 mm and sampled at a depth interval of 25 mm. All cone indexes were measured as shown in Fig. 3.

### 2.2.2. DEM soil modeling

EDEM\_v2020 was used to model the soil in the field test, where the base model between all the simulated materials was set as Hertz-Mindlin (no slip). The additional model between the particles was set as Hertz-Mindlin (no slip) with Bonding for mapping the physical properties of the field soil.

The cone index test was used to calibrate DEM parameters for modeling the simulated soil, which is an important index used to evaluate the soil compactness (Woldeyohannis et al., 2024; et al., 2000). As shown in Fig. 4, the simulated cone index test was established by using a cone with the same geometric dimensions and vertical velocity of 30 mm/s, following the ASAE standards (ASAE S313.3 FEB04/ASAE EP542), as it was in the field experimental test. A soil bin with a height of 280 mm and a total particle number of 15523 was generated in a 300 × 300 × 600 mm box in which the DEM parameters used were listed in Table 2 (Chen et al., 2024; Wang et al., 2023; Wu et al., 2021). In the simulation, the cone index value was obtained by dividing the vertical resistance of the cone by the area of its base. And the cone index when the cone was just completely submerged into the surface of the soil bin was considered to be the cone index of the soil bin at the depth of 0 cm.

The simulated cone indexes were recorded in the same way as for the field tests, with cone indexes recorded at a depth interval of 2.5 cm in depths of 0–10 cm. The parameters of the contact model were then iteratively updated until the simulated cone index had an acceptable error concerning that recorded in the field tests. It was found that generating the particles with a fixed radius was not a realistic approach for either particle packing or particle movement but this was able to be overcome by randomly generating particles in a size range of 0.95–1.05 times the nominal particle size (Ucguil et al., 2014). The calibrated parameters are listed in Table 2.

A 3000 × 600 × 210 mm soil bin was created for seeding simulation where the DEM parameters were used as listed in Table 2. In addition, two linearly scaled contact model parameters were used to model soils with different cone indexes, where the scaled parameters are listed in Table 3. The particle arrangement and total number of particles in these three soil bins were consistent because they were derived from the same DEM project file and differed only in the contact model parameters. The cone indexes of these soil bins are shown in Fig. 5.

### 2.3. Vibration analysis simulation test based on MBD-DEM coupling

During the operation of the no-tillage planter, the double disc furrow openers and GWs were rotated passively under the action of the soil,

**Table 1**

Physical properties of the soil sampling from the experimental field.

Soil Properties (Unit)	Value
Sampling depth (mm)	0–100
Water content (%)	6.79 ± 1.66
Wet density (kg·m <sup>-3</sup> )	1180.98 ± 46.23

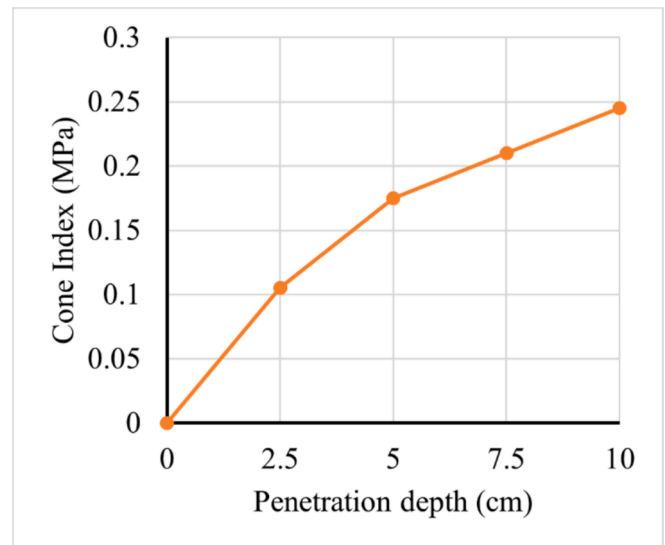


**Fig. 3.** Measurements of the cone indexes from the field experimental test.

which needs to be analyzed by the discrete element method. The total downforce of the NTSU was mainly provided by the deadweight and the downforce which exerted by the profiled springs. These forces are counteracted by vertical reactions force from the soil, applied to the double disc furrow openers and GW (Brune et al., 2018), and the interaction force is analyzed by the simulation of the furrowing process of the NTSU through the RecurDyn. However, the process of “furrowing – depth limitation – profiling” cannot be accomplished by single discrete element software and multibody dynamics software. Therefore, the coupled simulation of RecurDyn-EDEM was used for the relevant analysis.

#### 2.3.1. Simulation model of coupled furrowing operations

The core of the RecurDyn-DEM coupled model was the construction of the coupled furrowing operation, which included the process of “furrowing – depth limitation – profiling.”

The virtual prototype model of the NTSU was first imported into the RecurDyn software. The Joints, Springs, and Contacts were carried out to implement the process of “furrowing – depth limitation – profiling.” The Revolte and Fixed joints were added to the NTSU, which was used to realize the passive rotation. The Translate joint was added to the four-bar profiling device, and its direction along the z-axis was used to realize the linear motion of the NTSU. The Spring force was added to the four-bar profiling device to simulate the real mechanical spring. The spring parameters were selected based on the no-till planter in the field test. Then, the GeoSur contacts were added to the DLAHs, the GWSAs, and the compaction spring connecting frame, which was used to describe the contact collision. The stiffness and damping coefficient were calculated through the theoretical analysis in Section 2.2. Finally, the MBD model was imported into the DEM.

The material (steel, rubber) parameters were unified as listed in Table 4. The time steps of EDEM and RecurDyn were set to 5 × 10<sup>-5</sup> s and 1 × 10<sup>-3</sup> s, respectively; and the total time was 2.5 s. The NTSU begins to fall as the model runs, overcoming the trenching resistance through deadweight and downforce, thus achieving the process of “furrowing – depth limitation – profiling.” The working process diagram of the NTSU simulation model was shown in Fig. 6.

#### 2.3.2. Test design

According to the previous theoretical analysis, the interaction was understood through a three-factor, three-level orthogonal test. The working velocity( $X_1$ ), SSC( $X_2$ ), and cone index( $X_3$ ) were selected as factors. The factors and levels were shown in Table 5. A single factor test

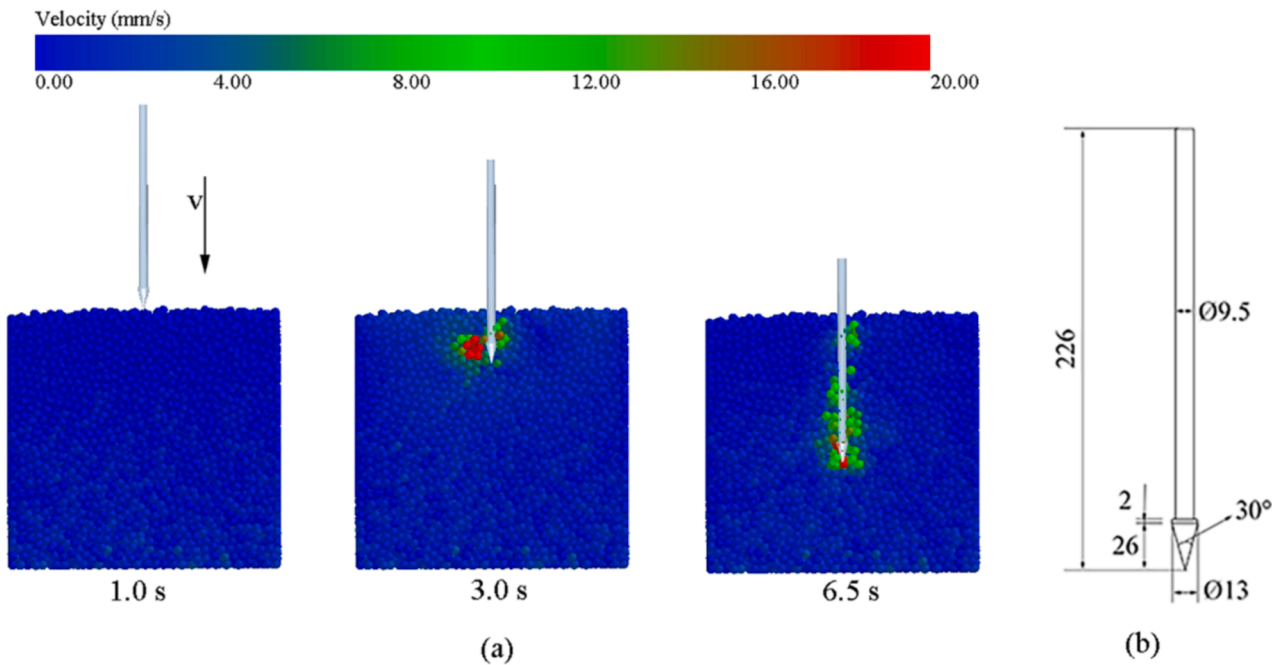


Fig. 4. (a) The simulated cone index test by using the discrete element method, (b) the penetration test tools (dimensions in mm).

Table 2

DEM parameters used in the simulated cone index test.

Properties (Unit)	Value
Physical radius of the soil particle (mm)	5
Contact radius of the soil particle (mm)	6
Density of the soil ( $\text{kg}\cdot\text{m}^{-3}$ )	1898
Shear modulus of the soil (Pa)	$7.9\text{e} + 5$
Poisson's ratio of the particle	0.38
Density of the steel ( $\text{kg}\cdot\text{m}^{-3}$ )	7850
Shear modulus of the steel (Pa)	$7.78\text{e} + 10$
Poisson's ratio of the steel	0.3
Restitution coefficient of the soil-soil	0.1
Static friction coefficient of the soil-soil	0.268
Rolling friction Coefficient of the soil-soil	0.2
Restitution coefficient of the soil-steel	0.5
Static friction coefficient of the soil-steel	0.5
Rolling friction Coefficient of the soil-steel	0.4
Fixed time step (s)	$5\text{e}-5$
Normal stiffness per unit area of soil-soil( $\text{N}\cdot\text{m}^{-3}$ )	$9\text{e} + 5$
Shear stiffness per unit area of soil-soil ( $\text{N}\cdot\text{m}^{-3}$ )	$9\text{e} + 5$
Critical normal stress of soil-soil (Pa)	$3\text{e} + 5$
Critical shear stress of soil-soil (Pa)	$3\text{e} + 5$

Table 3

The scaled parameters of contact model from the calibrated result.

Properties	Parameters	Scaled 1	Scaled 2
Soil-Soil (Hertz-Mindlin with Bonding)	Normal stiffness per unit area ( $\text{N}\cdot\text{m}^{-3}$ )	$5 \times 10^5$	$1.7 \times 10^6$
	Shear stiffness per unit area ( $\text{N}\cdot\text{m}^{-3}$ )	$5 \times 10^5$	$1.7 \times 10^6$
	Critical normal stress (Pa)	$2.0 \times 10^5$	$5.0 \times 10^5$
	Critical shear stress (Pa)	$2.0 \times 10^5$	$5.0 \times 10^5$

was used to validate the model, and the test factor was working velocity, which was consistent with the field test.

The seeding intensity, vertical force, and amplitude were selected as tests in indicators. The data could be collected during the stabilization phase of the vibration analysis simulation.

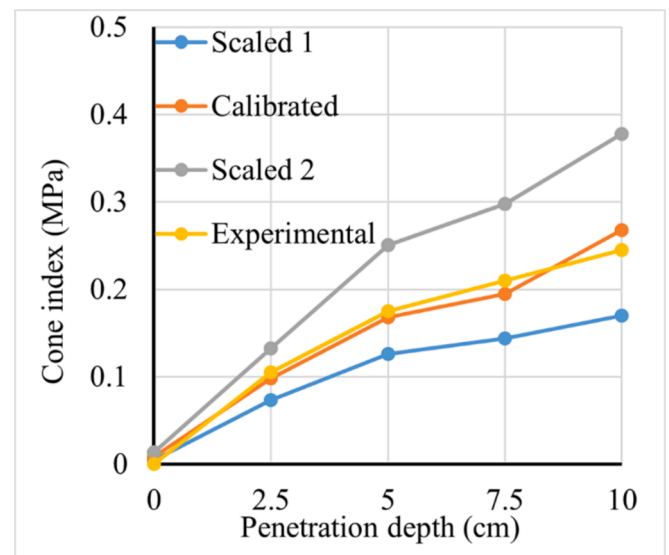


Fig. 5. The cone indexes of the simulated soil bins and field experimental tests.

Table 4

MBD-DEM parameters used in the vibration analysis simulation test.

Properties	Value
The stiffness coefficient of GeoSurContact	300,000
The damping coefficient of GeoSurContact	30
Density of the rubber ( $\text{kg}\cdot\text{m}^{-3}$ )	1130
Shear modulus of the rubber (Pa)	$7.966 \times 10^5$
Poisson's ratio of the rubber	0.475
Restitution coefficient of the soil-rubber	0.55
Static friction coefficient of the soil-rubber	0.88
Rolling friction coefficient of the soil-rubber	0.18

The seeding intensity was obtained from the relative position of the double disc furrow opener and the GW, and the trenching depth was obtained by the height difference. Trenching depth decreased with the

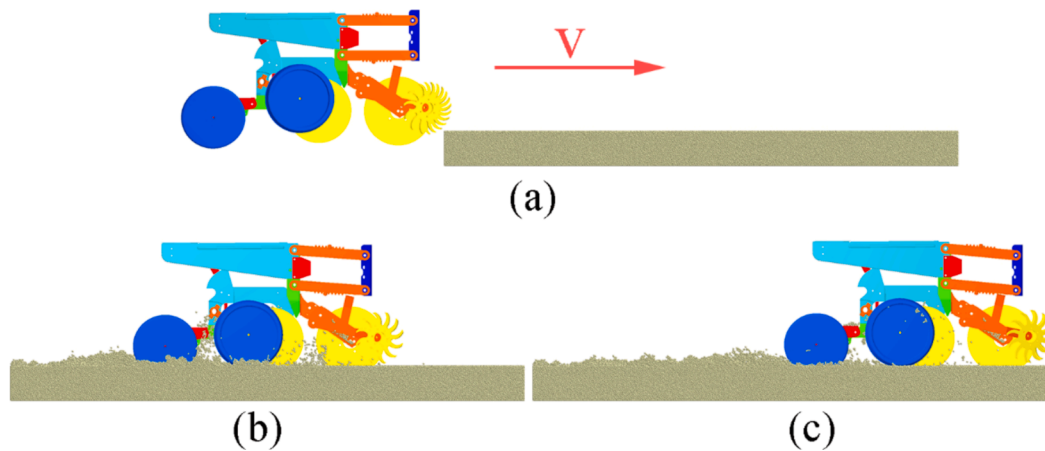


Fig. 6. The process of the vibration analysis simulation including the initial position (a), the stable operation (b), and the end position (c).

**Table 5**  
Test factor levels and code table.

Levels	Working velocity $X_1/(m \cdot s^{-1})$	Spring stiffness coefficient $X_2/(N \cdot mm^{-1})$	Cone index $X_3/(MPa)$
-1	1.39	2	0.12
0	1.94	6	0.18
1	2.5	10	0.25

seeding intensity, but the collision was caused by the collision of the DLAHs and the GWSAs. At the same time, the maximum seeding depth is reached. Therefore, the seeding intensity was selected as the test indicator to reflect the possibility of collision.

Meanwhile, mechanical tillage resistance affects crop seeding emergence and root growth (Hosseini et al., 2016), and some studies have found that the downforce can reflect the changes in soil tillage resistance to a certain extent (Brune et al., 2018). The total downforce are the deadweight of the no-tillage unit and any superimposed mechanical force from the profiling springs, these forces are counteracted by ‘up-force’ reactions from the soil (Brune et al., 2018). Additionally, the force balance considers only vertical forces. Therefore, the vertical force was calculated by the reaction force between the soil-engaging

components and the soil.

Moreover, the simulated frame displacements were recorded in the same way as for the field tests, and the Fast Fourier Transformation (FFT) technique was applied to the displacement data to isolate the frequency components for analysis. The amplitude and main frequency were obtained using Matlab R2023a software.

#### 2.4. Field test of the vibration

A no-tillage unit was used in the field experimental test, as shown in Fig. 7a. The test soil type is loam soil, with a moisture content of 6.79 % for 0–100 mm soil and a wet bulk density of  $1.18 \text{ kg} \cdot \text{m}^{-3}$ .

It was necessary to measure the vibration parameters of the seeding unit during the field tests to serve as a comparison term for the results of the coupled DEM-MBD simulations. A vibration test and modal analysis instrument (China Orient Institute of Noise & Vibration, Beijing, China) was used to measure the vibration characteristics of the seeding unit under operating conditions. This instrument was connected to 4 accelerometers, which were glued on the frames of the seeding units on both sides of the planter, as shown in Fig. 7b. Field tests at operating speeds of 5, 7, and 9 km/h were realized, at the accelerometer sampling frequency of 1000 hz. The data was processed by low-frequency filtering (0 ~ 50hz)

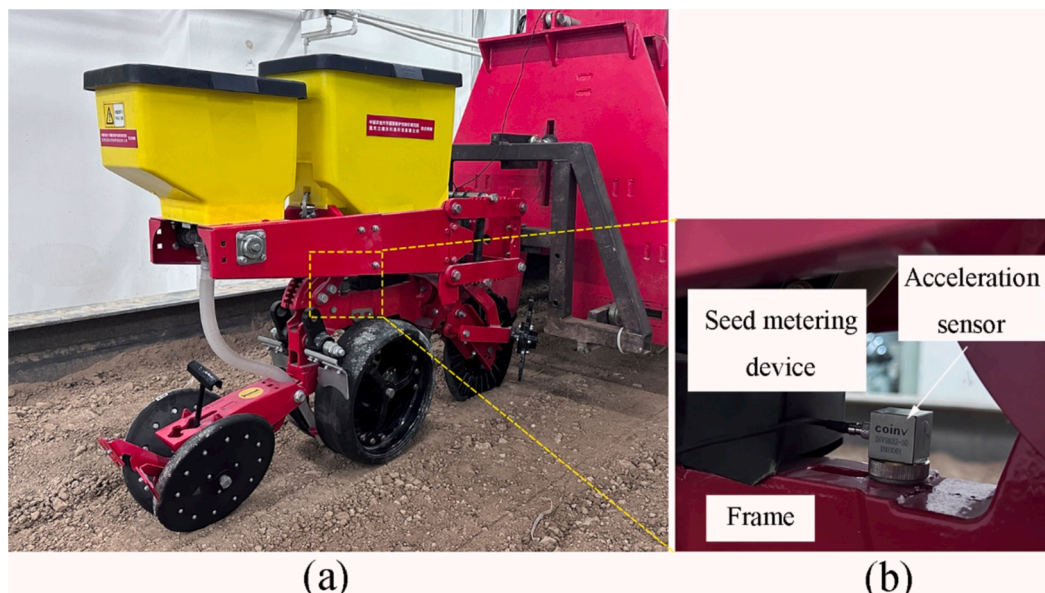


Fig. 7. (a) The no-tillage unit used in the field experimental test, and (b) the accelerometer glued on the frame of one of the no-tillage unit.

through the system's software, which was selected from the stabilization stage. The main frequency and amplitude data of the no-tillage planter were obtained using Matlab software.

### 3. Results

#### 3.1. Validation of the MBD-DEM coupling model

The simulation results of the working velocity for the MBD-DEM coupling model validation were shown in Fig. 8. It could be observed that the measured and simulated results closely match at the working velocity of 1.39 and 1.94 m/s, the maximum amplitude error was 1.42 and 3.49 mm, respectively. However, the error was 13.20 mm for the working velocity of 2.50 m/s. This was probably due to the fact that the total weight of the no-till seeding monomer was reduced after simplification, and the downforce of the no-tillage unit was not enough to reach the ideal furrowing depth. In addition, the vibration frequencies of simulation results concentrated mainly in a low frequency from 4 to 10 Hz, which was consistent with the actual results. It meant that the completeness of the MBD-DEM modeling of the no-tillage unit that reflected the real-scale agricultural working environment could be implemented with a meaningful level of accuracy.

In summary, the coupled simulation technology based on MBD-DEM could analyze the vibration characteristics of no-tillage seeding units, which was a completely new approach.

#### 3.2. Effects of parameters on seeding intensity

The seeding intensity increased with the decrease in seeding depth, which reflected the change in sowing depth and the possibility of collision. At the same time, the maximum seeding depth was obtained at the minimum seeding intensity. As shown in Fig. 9, the seeding intensity increased with the increase in working velocity, which may be due to the higher collision incidence between the GWSA and the DLAH at high velocity. In other words, the higher seeding intensity produced a high vibration, which means that a higher rate of seeding depth variation will

be generated.

When the working velocity was the lowest (Fig. 9a), the seeding intensity increased as cone index increased, which indicated that soil compaction had a more significant effect on the seeding intensity. However, when the working velocity is high (Fig. 9b, c), the low cone index performed better, indicating that in the case of more compact soil, it was necessary to provide a sufficiently large downforce to reduce the seeding intensity and thus improve the seeding quality.

The coordinates of the double disc furrow openers and the GW in the Y-direction were obtained by numerical modeling, which better simulated and described the change of seeding intensity in the "furrowing – depth limitation – profiling" process of NTSU. The test scheme and results were listed in Table 6.

#### 3.3. Effects of parameters on vertical force

The vertical force mainly depended on cone index. When cone index was low, the vertical fluctuated little and remained at a low level, but unreasonable operating parameters will lead to large fluctuations in trenching resistance as shown in Fig. 10. This was probably due to the fact that the double disc furrow opener relies on the unit's deadweight, and the downforce of the profiling springs was not enough to reach the ideal furrowing depth. In addition, the difference between the average vertical force was smaller (Fig. 10a); this may be due to the need for more significant unit deadweight and downforce to overcome furrowing resistance in the case of high soil compactness (Sharipov et al., 2018), which may otherwise result in shallower seeding depths (Fig. 10c). The constant total downforce is insufficient for the opening disc to cut to the desired depth, then the seed would be planted too shallow, which is an undesirable agronomic outcome (K. E. Lamb & Johnson, 2004).

The fluctuation of vertical force was small (Fig. 10a), which indicated that in the case of lower soil compactness, the working velocity and SSC (downforce) had less influence on it, and it could be stabilized in a reasonable range. It could be seen that the fluctuation of the furrowing resistance of test 13 (2.5 m/s, 6 N/mm, and 0.25 MPa) was more significant (Fig. 10b), which indicated that in the case of more

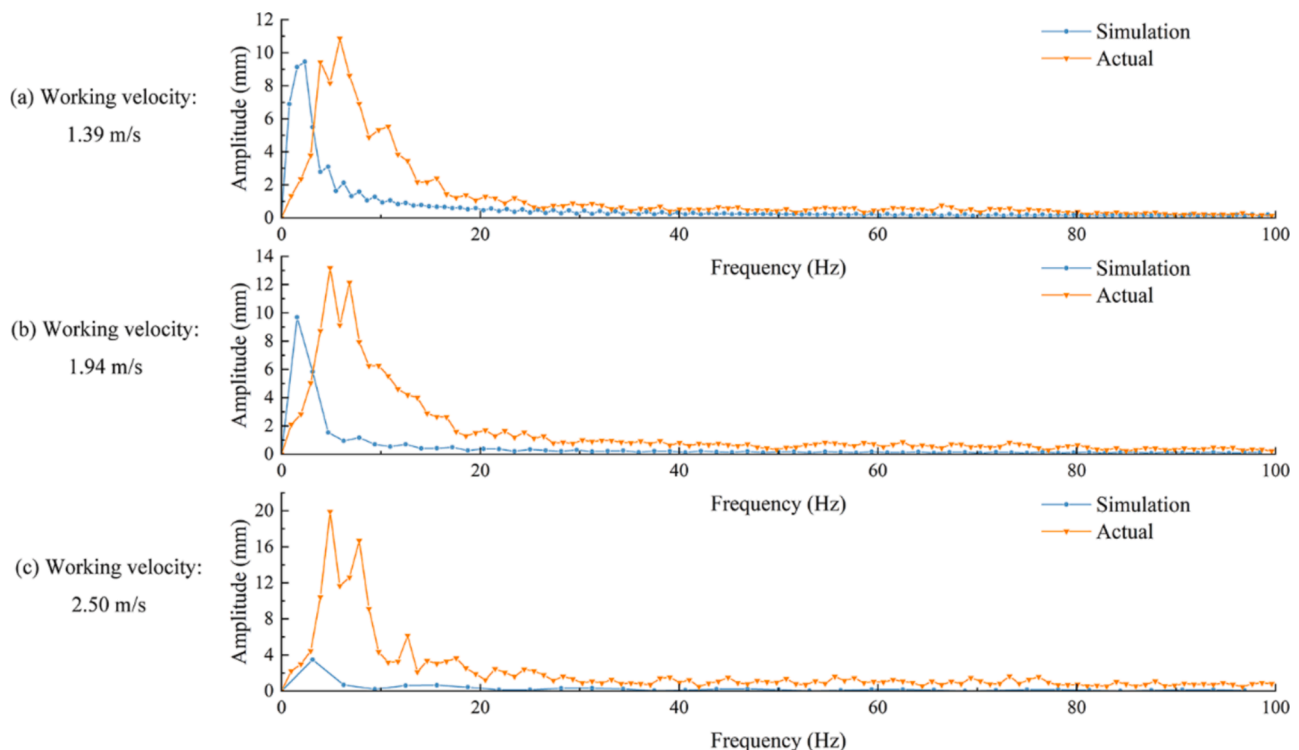
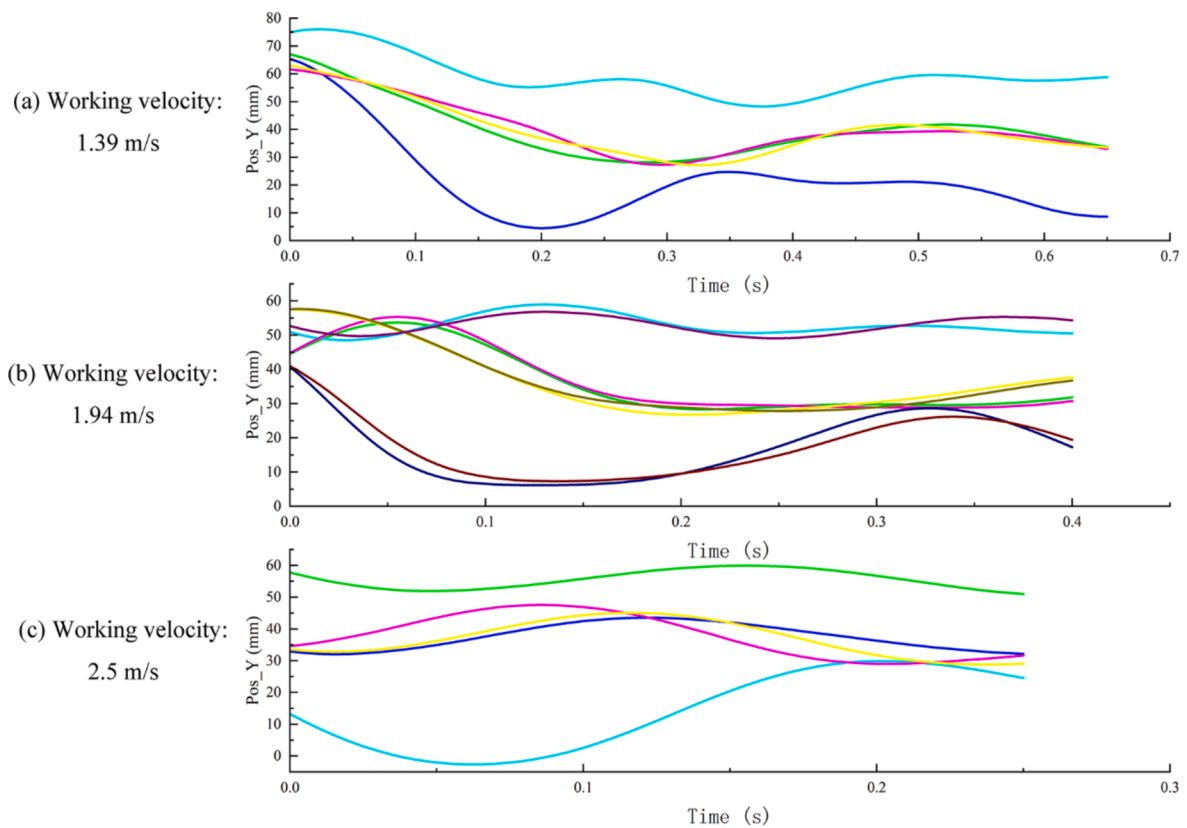


Fig. 8. The comparison of simulation and actual with a working velocity of 1.39 m/s, 1.94 m/s, and 2.50 m/s, respectively.



**Fig. 9.** The effect of working velocity, spring stiffness coefficient and cone index on seeding intensity. (a) The green, blue, cyan, carmine, and yellow line is the test 10, 12, 15, 16, and 19, respectively; (b) The green, blue, cyan, carmine, yellow, deep yellow, navy blue, purple, and wine red line is the test 1, 2, 4, 6, 7, 8, 9, 11, and 14, respectively; (c) The green, blue, cyan, carmine, and yellow line is the test 3, 5, 13, 17, and 18, respectively.

**Table 6**  
Design and results of tests.

Test No.	Working velocity $X_1/$ (m·s <sup>-1</sup> )	Spring stiffness coefficient $X_2/$ (N·mm)	Cone index $X_3/$ (MPa)	Average seeding intensity $Y_1/$ mm	Vertical force $Y_2/$ N	Maximum amplitude $Y_3/$ mm
1	1.94	6	0.18	36.44	998.68	8.76
2	1.94	6	0.18	36.80	995.36	9.69
3	2.50	6	0.12	55.60	984.99	1.68
4	1.94	10	0.12	52.86	989.48	2.51
5	2.50	10	0.18	37.51	1020.66	2.82
6	1.94	6	0.18	36.80	995.36	9.69
7	1.94	6	0.18	36.80	999.54	9.15
8	1.94	6	0.18	36.47	1004.11	9.49
9	1.94	2	0.25	17.34	994.81	9.88
10	1.39	10	0.25	39.76	1015.91	9.71
11	1.94	2	0.15	52.91	988.09	0.97
12	1.39	6	0.25	21.57	991.45	11.32
13	2.5	6	0.25	13.80	939.82	11.48
14	1.94	10	0.25	17.58	1000.59	9.40
15	1.39	6	0.12	58.98	989.41	7.65
16	1.39	2	0.18	40.26	1009.76	9.69
17	2.5	2	0.18	37.79	1011.60	3.26
18	2.5	6	0.18	36.88	1019.28	3.49
19	1.39	6	0.18	39.85	1012.74	6.89

significant cone index, it was necessary to choose the working velocity and downforce reasonably.

3.4. Effects of parameters on the maximum amplitude of the unit

The Post Result of RecurDyn was used to output the frame vertical coordinate data, which was analyzed using the FFT spectrum by Matlab. The results are shown in Fig. 11. There was a close correlation between sowing intensity and amplitude, as shown in Figs. 9, and 11. At low

working velocity, the maximum amplitude increased as the working velocity increased. However, the maximum amplitude can be reduced effectively due to reasonable operation parameter settings, which include the SSC and cone index.

According to previous research, the main frequencies of the vibration were concentrated in a low frequency band from 0 to 10hz(Zhai et al., 2020). The main vibration frequencies of simulation test were not increased with the increase in working velocity but remained at 1.56, 2.34, and 3.13hz (Fig. 11a, b, and c). In specific, maximum amplitudes

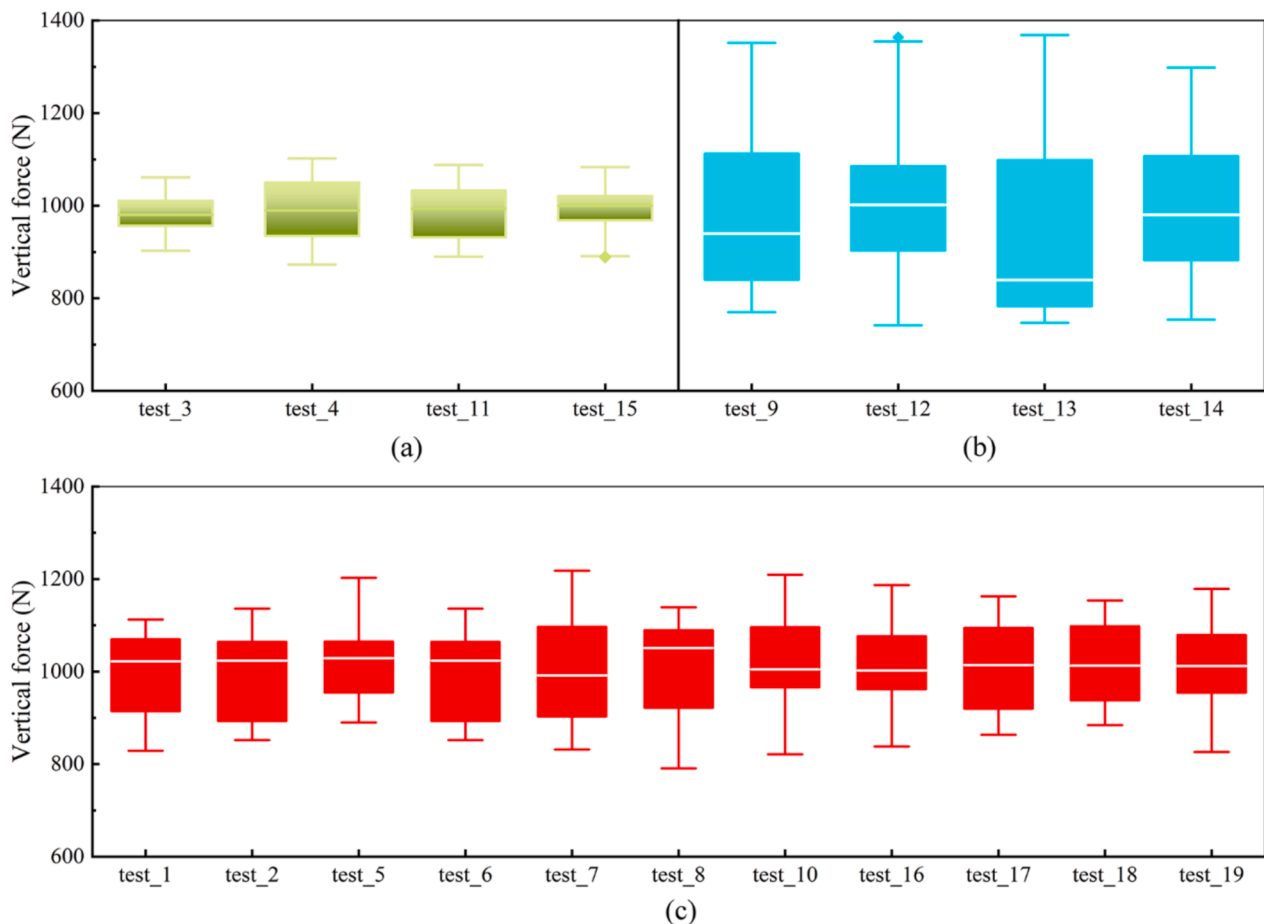


**Fig. 10.** The effect of working velocity, spring stiffness coefficient and cone index on vertical force. (a) (b) (c) the cone indexes of 0.12, 0.25, and 0.18 MPa, respectively.

under 1.39 m/s were 9.71, 11.32, 7.65, 8.58, and 9.46 mm, which did not change significantly. Compared with the other treatment groups, the maximum amplitude of test 4, and test 11 (Fig. 11b) was significantly lower than that of the others. This phenomenon is explained by the current total downforce is sufficient to meet the needs of trenching. Moreover, compared to the other treatment groups, the maximum amplitude was significantly lower under 2.5 m/s (Fig. 11c), which is inconsistent with the previous results. Therefore, the higher working velocity should be avoided when the downforce is insufficient in the case for no-tillage seeding. Alternatively, it can be solved by replacing the mechanical spring with a higher stiffness coefficient or using an active downforce control system to increase the underground downforce.

#### 4. Discussion

In this study, a vibration model of the depth-limiting device was established, and a coupled dynamic simulation of MBD-DEM was established based on it; we analyzed the effects of working velocity, profiling SSC, and cone index on the vibration of the unit. The main novelty value of the research is the development of a coupling simulation combining the DEM and the MBD for the analysis of the vibration characteristics of no-tillage seeding unit. It is a completely new approach that can be used for vibration analysis of other mechanical systems.

It has shown that planter downforce has the potential to meaningfully describe distributions of soil strength in agricultural fields (Brune et al., 2018). These indicated vertical force had the potential to meaningfully describe the magnitude of soil strength in the simulation test. Under the condition of low soil compactness, the fluctuation of vertical force was smaller (Fig. 10). However, the cone index had no significant

effect ( $P > 0.05$ ) on the amplitude of the no-tillage unit. Therefore, the larger amplitude in no-tillage fields may be caused by soil surface roughness (Mohammadi et al., 2023). Furthermore, as the study was carried out only in loam soil, in order to better understand the interaction between passively vibrating tillage equipment and the soil, different velocities, different soil surface roughness, and downforce control systems could also be investigated in future studies.

#### 5. Conclusions

In this study, the soil-machine interaction (no-tillage unit) was modeled based on working velocity, soil cone index, and spring stiffness coefficient using the MBD-DEM coupling method to analyze the vibration characteristics during furrowing operation, and verified by comparison with field measurement data. Moreover, based on the following conclusions can be drawn:

Soil strength was an influential quantity in determining agricultural outcomes. The cone index test was used to calibrate DEM parameters for modeling the simulated soil, which was used to study the effect of soil compaction on the vibration of the no-tillage unit.

In the simulations, it was observed that working velocity was the main factor influencing the vibration of the no-tillage unit. However, it would also be affected by the downforce and the compactness of the soil. The maximum amplitude increased as the working velocity increased, but the main frequencies of the vibration were concentrated in a low frequency band from 0 to 10 Hz. Reasonable working velocity and profiling SSC (downforce) would be the main factors influencing the vibration of the no-tillage planter, which could effectively reduce the vibration of the seeding unit and improve the seeding quality.

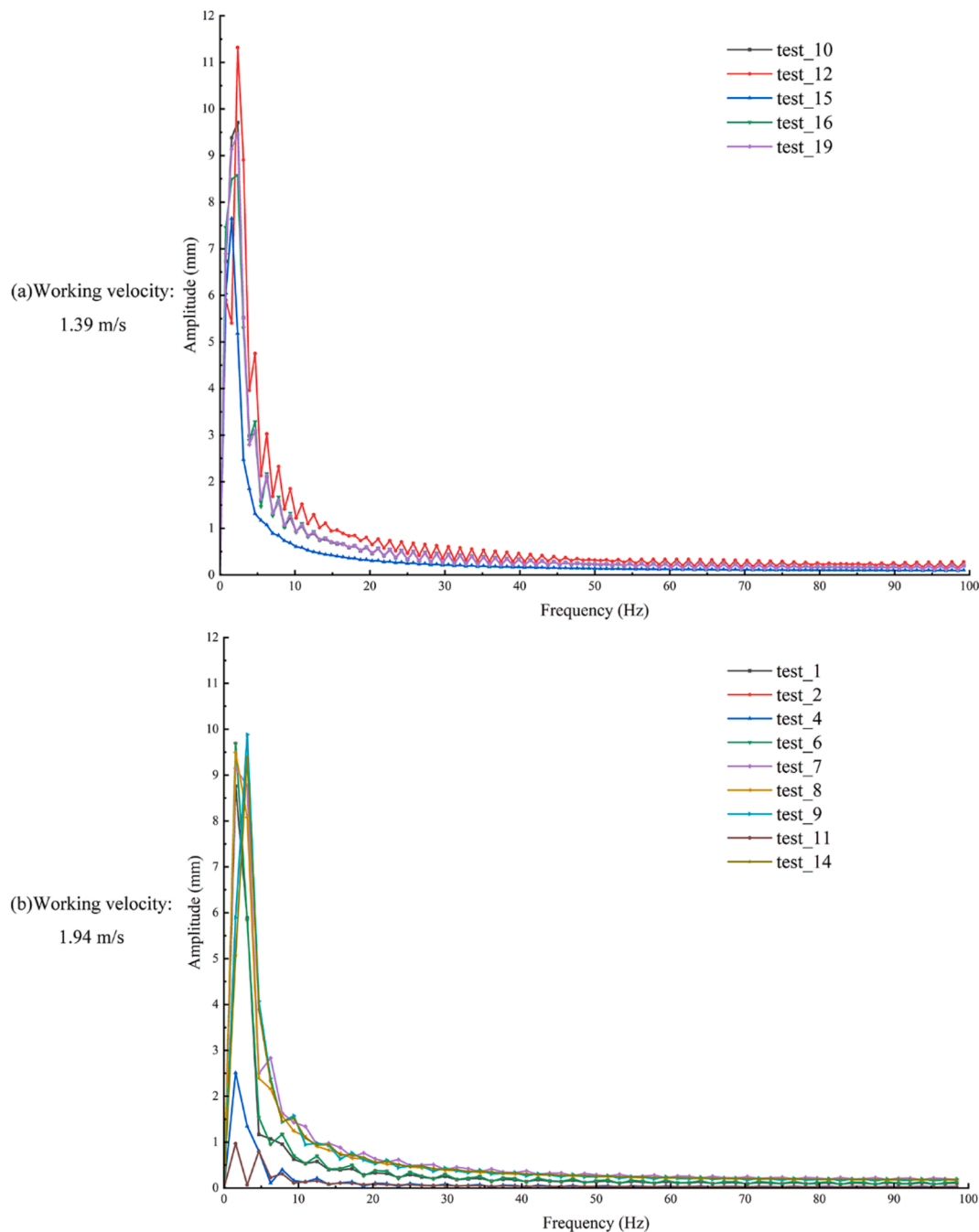


**Fig. 11.** The effect of working velocity, spring stiffness coefficient and cone index on maximum amplitude of simulation test. (a) (b) (c) the working velocity of 1.39, 1.94, and 2.50 m/s, respectively.

The MBD-DEM coupled simulation technology was used to analyze the vibration characteristics of no-tillage seeding units, as the coupled MBD-DEM simulations showed good agreement with the results from actual measurements.

This study provided a method for analyzing the vibration characteristics of no-tillage seeding units based on the MBD-DEM coupling, and provided a theoretical basis for the optimization design of the vibration damping system.

**CRedit authorship contribution statement**

**Dong He:** Writing – original draft, Software, Methodology, Investigation, Formal analysis, Conceptualization. **Hongwen Li:** Writing –

review & editing, Supervision, Resources, Funding acquisition, Conceptualization. **Jin He:** Writing – review & editing, Investigation, Funding acquisition. **Caiyun Lu:** Writing – review & editing, Investigation, Funding acquisition. **Chao Wang:** Writing – review & editing, Investigation, Funding acquisition. **Yingbo Wang:** Writing – review & editing, Investigation. **Zhengyang Wu:** Writing – review & editing, Validation, Software, Investigation. **Zhenwei Tong:** Visualization, Investigation. **Zhen Gao:** Visualization, Investigation.

**Declaration of competing interest**

The authors declare that they have no known competing financial interests or personal relationships that could have appeared to influence

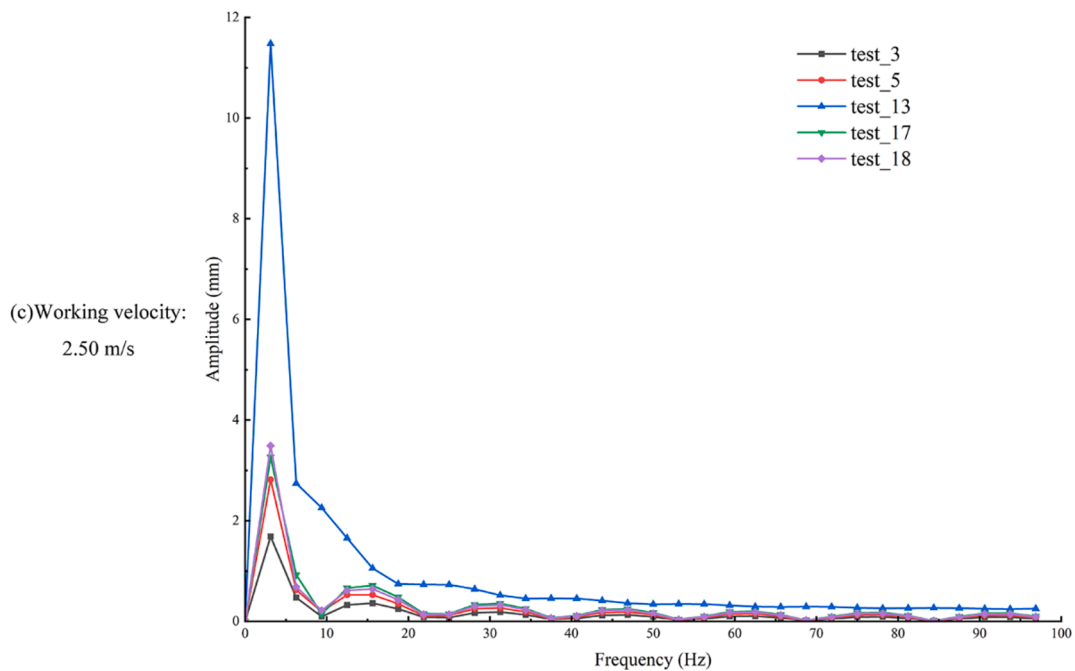


Fig. 11. (continued).

the work reported in this paper.

### Acknowledgements

This research was funded by the National Key Research and Development Program of China [Grant No. 2022YFD1500902] and the China Agriculture Research System of MOF and MARA [Grant No. CARS-03], and the National Natural Science Foundation of China [Grant No. 32201674], and the 2115 Talent Development Program of China Agricultural University and Chinese Universities Scientific Fund [Grant No. 2021TC105].

### Data availability

Data will be made available on request.

### References

- Amir Kassam, T.F.F.S., 2009. The spread of Conservation Agriculture justification, sustainability and uptake. *Int. J. Agric. Sustain.* 7 (4), 292–320. <https://doi.org/10.3763/ijas.2009.0477>.
- Badua, S.A., Sharda, A., Strasser, R., Ciampitti, I., 2021. Ground speed and planter downforce influence on corn seed spacing and depth. *Precision Agriculture* 22 (4), 1154–1170. <https://doi.org/10.1007/s11119-020-09775-7>.
- Brune, P.F., Ryan, B.J., Technow, F., Myers, D.B., 2018. Relating planter downforce and soil strength. *Soil Tillage Res.* 184, 243–252. <https://doi.org/10.1016/j.still.2018.08.003>.
- Cay, A., Kocabiyyik, H., May, S., 2018. Development of an electro-mechanic control system for seed-metering unit of single seed corn planters Part I: Design and laboratory simulation. *Computers and Electronics in Agriculture* 144, 71–79. <https://doi.org/10.1016/j.compag.2017.11.035>.
- Chen, G., Wang, Q., Li, H., He, J., Wang, X., Zhang, X., He, D., 2024. Experimental research on vertical straw cleaning and soil tillage device based on Soil-Straw composite model. *Computers and Electronics in Agriculture* 216, 108510. <https://doi.org/10.1016/j.compag.2023.108510>.
- J. L. Hernanz, H. Peixoto, C. Cerisola, V. S. (2000). An empirical model to predict soil bulk density profiles in field conditions using penetration resistance, moisture content and soil depth. *Journal of Terramechanics*, 37(4), 167–184. [http://doi.org/10.1016/S0022-4898\(99\)00020-8](http://doi.org/10.1016/S0022-4898(99)00020-8).
- Hosseini, M., Movahedi Naeini, Dehghani, A.A., Khaledian, Y., 2016. Estimation of soil mechanical resistance parameter by using particle swarm optimization, genetic algorithm and multiple regression methods. *Soil and Tillage Research* 157, 32–42. <https://doi.org/10.1016/j.still.2015.11.004>.
- Hunt, K., Crossley, E., 1975. Coefficient of restitution interpreted as damping in vibroimpact. *Journal of Applied Mechanics* 45 (2), 440–445. <https://doi.org/10.1115/1.3423596>.
- Kassam, A.H.F.T., 2015. Overview of the worldwide spread of conservation agriculture. *Field Actions Science Reports* 8, 1–11.
- Kirkegaard Nielsen, S., Munkholm, L.J., Lamandé, M., Nørremark, M., Skou-Nielsen, N., Edwards, G.T.C., Green, O., 2017. Seed drill instrumentation for spatial coulters depth measurements. *Computers and Electronics in Agriculture* 141, 207–214. <https://doi.org/10.1016/j.compag.2017.07.014>.
- Lamb, K.E., Johnson, B.L., 2004. Seed size and seeding depth influence on canola emergence and performance in the northern great plains. *Agron. J.* 96, 454–461.
- Liu, Y., Zhao, M., Liu, F., Dong, S., Zhang, X., 2015. Vibration test and analysis of no-tillage planter on the maize stubble surface. *Adv. Mat. Res.* 1061–1062, 788–793. <https://doi.org/10.4028/www.scientific.net/AMR.1061-1062.788>.
- Machado, M., Moreira, P., Flores, P., Lankarani, H.M., 2012. Compliant contact force models in multibody dynamics: evolution of the Hertz contact theory. *Mechanism and Machine Theory* 53, 99–121. <https://doi.org/10.1016/j.mechmachtheory.2012.02.010>.
- Mohammadi, F., Maleki, M.R., Khodaei, J., 2023. Laboratory evaluation of infrared and ultrasonic range-finder sensors for on-the-go measurement of soil surface roughness, 105678 *Soil Tillage Res.* 229. <https://doi.org/10.1016/j.still.2023.105678>.
- Pásthy, L., József Farkas, Z., Haba, T., Tamás, K., 2024. Development of a multi-way coupled discrete-finite element method simulation procedure for modelling soil-passive vibration tool interaction, 108459 *Comput. Electron. Agric.* 216. <https://doi.org/10.1016/j.compag.2023.108459>.
- Ramírez, R., Pöschel, T., Brilliantov, N.V., Schwager, T., 1999. Coefficient of restitution of colliding viscoelastic spheres. *Phys. Rev. E* 60 (4), 4465.
- Rodrigues Da Silva, M., Marques, F., Tavares Da Silva, M., Flores, P., 2022. A compendium of contact force models inspired by Hunt and Crossley's cornerstone work, 104501 *Mech. Mach. Theory* 167. <https://doi.org/10.1016/j.mechmachtheory.2021.104501>.
- Sharipov, G.M., Paraforos, D.S., Pulatov, A.S., Griepentrog, H.W., 2017. Dynamic performance of a no-till seeding assembly. *Biosyst. Eng.* 158, 64–75. <https://doi.org/10.1016/j.biosystemseng.2017.03.016>.
- Sharipov, G.M., Paraforos, D.S., Griepentrog, H.W., 2018. Implementation of a magnetorheological damper on a no-till seeding assembly for optimising seeding depth. *Comput. Electron. Agric.* 150, 465–475. <https://doi.org/10.1016/j.compag.2018.05.024>.
- Tsuji Y, Tanaka T, T, I. (1992). Lagrangian numerical simulation of plug flow of cohesionless particles in a horizontal pipe. *Powder Technology*, 71(3), 239–250.
- Skrinjar, L., Slavič, J., Boltežar, M., 2018. A review of continuous contact-force models in multibody dynamics. *International Journal of Mechanical Sciences* 145, 171–187. <https://doi.org/10.1016/j.ijmecsci.2018.07.010>.
- Ucgul, M., Fielke, J.M., Saunders, C., 2014. Three-dimensional discrete element modelling of tillage: Determination of a suitable contact model and parameters for a cohesionless soil. *Biosyst. Eng.* 121, 105–117. <https://doi.org/10.1016/j.biosystemseng.2014.02.005>.
- Virk, S.S., Porter, W.M., Li, C., Rains, G.C., Snider, J.L., Whitaker, J.R., 2021. On-farm evaluation of planter downforce in varying soil textures within grower fields. *Precis. Agric.* 22 (3), 777–799. <https://doi.org/10.1007/s11119-020-09755-x>.
- Wang, G., Liu, C., 2020. Further investigation on improved viscoelastic contact force model extended based on hertz's law in multibody system, 103986 *Mech. Mach. Theory* 153. <https://doi.org/10.1016/j.mechmachtheory.2020.103986>.

- Wang, J., Xu, Y., Wang, C., Xiang, Y., Tang, H., 2023. Design and simulation of a trenching device for rice straw burial and trenching based on MBD-DEM. *Computers and Electronics in Agriculture* 207, 107722. <https://doi.org/10.1016/j.compag.2023.107722>.
- Wang, Q., Zhu, L., Li, M., Huang, D., Jia, H., Zhuang, J., 2019. Vibration characteristics of corn no-tillage finger-type precision planter and its effect on seeding performance. *Trans. Csaе* 35 (9), 9–18.
- Woldeyohannis, Y. S., S Hiremath, S., Tola, S., Wako, A. (2024). Influence of soil physical and chemical characteristics on soil compaction in farm field. *Heliyon*, 10(3), e25140. <http://doi.org/10.1016/j.heliyon.2024.e25140>.
- Wu, Z., Wang, X., Liu, D., Xie, F., Ashwehmbom, L.G., Zhang, Z., Tang, Q., 2021. Calibration of discrete element parameters and experimental verification for modelling subsurface soils. *Biosystems Engineering* 212, 215–227. <https://doi.org/10.1016/j.biosystemseng.2021.10.012>.
- Zhai, C., Long, J., Taylor, R., Weckler, P., Wang, N., 2020. Field scale row unit vibration affecting planting quality. *Precision Agriculture* 21 (3), 589–602. <https://doi.org/10.1007/s11119-019-09684-4>.
- Zhang, X., Li, C., Li, J., Zou, M., 2014. Mathematic vibration model of spade punch planter of maize. *Trans.Chin. Soc. Agric. Mach* 45, 88–93.
- Zhang, J., Liang, X., Zhang, Z., Feng, G., Zhao, Q., Zhao, L., He, G., 2022. A continuous contact force model for impact analysis. *Mechanical Systems and Signal Processing* 168, 108739. <https://doi.org/10.1016/j.ymssp.2021.108739>.
- Zhang, T., Liu, F., Zhao, M., Liu, Y., Li, F., Chen, C., Zhang, Y., 2016. Movement law of maize population in seed room of seed metering device based on discrete element method. *Chinese Soc Agric. Eng.* 32, 27–35. <https://doi.org/10.11975/j.issn.1002-6819.2016.22.004>.